Author Manuscript

Author Manuscript

Author Manuscript

Author Manuscript

HHS Public Access

Author manuscript

Nat Comput Sci. Author manuscript; available in PMC 2024 April 06.

Published in final edited form as:

Nat Comput Sci. 2023 April ; 3(4): 291–300. doi:10.1038/s43588-023-00422-5.

Exploring Proton-Coupled Electron Transfer at Multiple Scales

Sharon Hammes-Schiffer

Department of Chemistry, Yale University, New Haven, CT 06520

Abstract

The coupling of electron and proton transfer is critical for chemical and biological processes spanning a wide range of length and time scales and often occurring in complex environments. Thus, diverse modeling strategies, including analytical theories, quantum chemistry, molecular dynamics, and kinetic modeling, are essential for a comprehensive understanding of such proton-coupled electron transfer reactions. Each of these computational methods provides one piece of the puzzle, and all these pieces must be viewed together to produce the full picture.

1. Introduction

Proton-coupled electron transfer (PCET), which is defined broadly as the coupled motion of electrons and protons, is vital to a wide range of chemical and biological processes.[1–4] Multiscale modeling strategies are required to study these processes because they occur over an extensive range of length and time scales. A combination of analytical theories, quantum chemistry methods, molecular dynamics (MD) simulation approaches, and kinetic modeling schemes has been used to investigate PCET reactions in various complex environments. The modeling of PCET at electrochemical interfaces has been reviewed recently.[5] Thus, this Perspective will focus on PCET in solution and proteins, describing illustrative examples of how various computational approaches can be combined to obtain fundamental insights about chemically and biologically important systems, such as electrocatalysts, photocatalysts, enzymes, and photoreceptors. The feedback between computational and experimental studies will also be emphasized through these examples.

The workhorse for computational studies of PCET is density functional theory (DFT), although higher levels of theory, such as multireference wavefunction methods, may be used to attain more quantitative accuracy. DFT can be used for ground state geometry optimizations and the calculation of relative free energies, which are directly related to experimentally measurable proton-coupled redox potentials and driving forces. To study photoinduced PCET reactions, excited state methods such as time-dependent DFT (TDDFT)[6] or multireference wavefunction methods[7] can be used to optimize geometries in excited states and to calculate absorption and emission energies related to experimental

sharon.hammes-schiffer@yale.edu .

Author Contributions:

There is only one author.

Competing Interests:

The author declares no competing interests.

Author Manuscript Author Manuscript Author Manuscript Author Manuscript

measurements.[8, 9] To investigate the real-time dynamics of PCET reactions, MD trajectories can be propagated on either ground or excited state potential energy surfaces. Nonadiabatic dynamics methods such as Ehrenfest[10] or surface hopping[11] can be used to propagate trajectories on multiple surfaces. For larger systems such as proteins, hybrid quantum mechanical/molecular mechanical (QM/MM) methods allow only the portion of the system undergoing chemistry to be treated quantum mechanically with a method such as DFT, while the remaining atoms are treated with a molecular mechanical force field. These types of simulations provide useful mechanistic information about complex processes.

In addition to these computational methods, a general theoretical formulation of PCET[12–14] provides a conceptual framework and analytical rate constant expressions. This theory treats the transferring proton(s), as well as the electrons, quantum mechanically and thereby accounts for hydrogen tunneling, which plays a significant role in many PCET reactions. In the vibronically nonadiabatic regime, concerted PCET reactions are described in terms of nonadiabatic transitions between two sets of electron-proton vibronic states. Analogous to Marcus theory for electron transfer,[15] a solvent fluctuation leads to the degeneracy between a pair of reactant and product vibronic states, and the electron and proton tunnel simultaneously with a probability determined by the square of the vibronic coupling. As shown in Eq. (1) below, the analytical nonadiabatic PCET rate constant expression sums over all reactant and product vibronic states, where each term in the double summation depends exponentially on a free energy barrier expressed in terms of the reaction free energy and reorganization energy and is weighted by the square of the vibronic coupling. The input quantities such as reaction free energy, reorganization energy, and vibronic coupling can be computed with DFT and other computational techniques.

The remainder of this Perspective presents examples that showcase the use of diverse strategies on multiple scales to investigate different types of PCET reactions. For PCET in molecular systems, both electrochemically and photochemically induced PCET reactions are discussed. For PCET in enzymes, an enzyme catalyzing a single PCET reaction and an enzyme catalyzing multiple coupled PCET reactions are examined. The blue-light using flavin (BLUF) photoreceptor protein is presented as the final example of photoinduced PCET in a complex photocycle. Each of these examples illustrates the power of computation in revealing fundamental insights and stimulating experimental investigations. Many other computational studies of PCET[16–19] have provided significant insights and further illustrate the diversity of computational strategies.

II. PCET in molecular systems

PCET in molecular systems can be thermally activated or induced electrochemically or photochemically. This section will discuss an example of electrochemically induced PCET in benzimidazole-phenol (BIP) molecules and photochemically induced PCET in anthracene-phenol-pyridine triads. Both of these molecular systems were inspired by chemical steps in photosynthesis, and therefore understanding their mechanisms has implications for designing solar energy conversion devices.

Author Manuscript Author Manuscript Author Manuscript Author Manuscript

A. Electrochemically induced PCET in BIP molecules

Photosystem II is a central protein in photosynthesis that splits water into hydrogen and oxygen. A key step in the mechanism of photosystem II is PCET within a tyrosine-histidine pair, where oxidation of the tyrosine induces proton transfer from tyrosine to histidine.[20, 21] Computational studies have aided the design of a series of BIP systems inspired by this biological motif using benzimidazole to represent histidine and phenol to represent tyrosine (Figure 1).[22, 23] Moreover, these BIP systems have been extended to create proton wires that undergo multi-proton PCET processes for long-range proton translocation via a Grotthuss-type mechanism.[24] Such proton wires were inspired by bioenergetic processes in which protons are pumped across a membrane to generate a potential difference that is vital to providing energy in living systems. Understanding the fundamental mechanisms of these processes is critical for controlling and tuning the biological systems as well as for designing artificial photosynthetic systems.

A variety of computational methods have been applied to these molecular systems. Each of these computational methods has provided distinct insights into the physical principles underlying these PCET processes. For example, DFT calculations were used to compute proton-coupled redox potentials,[22, 23, 25] which agree with experimental data, and to design systems that transport multiple protons over hydrogen-bonded networks,[24] where an E*n*PT process corresponds to a PCET reaction involving the transfer of *n* protons. Such DFT calculations predicted that the redox potential for an E2PT process would be significantly less positive than the redox potential for the analogous E1PT process, as subsequently verified experimentally (Figure 1A).[22] Moreover, another combined experimental and theoretical study produced BIP systems with substituents that mitigate the drop in redox potential (Figure 1A).[23] This ability to tune the redox potentials is important in the context of artificial photosynthesis. Subsequent studies designed E4PT systems that transported protons over ~16 Å (Figure 1B).[24]

In addition, vibronically nonadiabatic PCET theory[12–14] was used to compute the kinetic isotope effect (KIE), which is the ratio of the rate constants for hydrogen and deuterium. High KIEs are generally understood to implicate hydrogen tunneling,[26–28] although hydrogen tunneling has also been shown to be significant for systems with low KIEs.[22] The rate constant for an E1PT process has the following form[12–14]

$$k(R) = \sum_{\mu} P_{\mu} \sum_{\nu} \frac{\left|V^{\mathrm{el}} S_{\mu\nu}\right|^2}{\hbar} \sqrt{\frac{\pi}{\lambda k_B T}} exp\left[-\frac{(\Delta G^{\circ}_{\mu\nu} + \lambda)^2}{4\lambda k_B T}\right] \quad (1)$$

$$k = \int P(R) k(R) dR \quad (2)$$

where the summations are over reactant and product vibronic states, P_{μ} is the Boltzmann population of reactant state μ, V^{el} is the electronic coupling, $S_{\mu\nu}$ is the overlap integral between reactant and product proton vibrational wavefunctions states μ and υ, λ is the reorganization energy, and $\Delta G^{\circ}_{\mu\nu}$ is the free energy of reaction for vibronic states μ and υ.

Author Manuscript Author Manuscript Author Manuscript Author Manuscript

Moreover, $\hbar$ is Planck's constant divided by 2π, k_B is the Boltzmann constant, and T is the temperature. In these equations, $k(R)$ is the rate constant at a proton donor-acceptor distance R, and Eq. (2) corresponds to the thermal averaging over the proton donor-acceptor distance R, where the rate constant for each R is weighted by the probability $P(R)$ of sampling this value of R. The same expression is applicable to EnPT processes involving n proton transfer reactions, although determination of the input quantities such as the overlap integrals requires the calculation of multidimensional proton vibrational wavefunctions.[22, 29]

In the application of this theory to the BIP systems, the input quantities were computed with DFT and other computational techniques. Note that the overlap integral is dependent on the proton potential energy surface, which in turn depends on the level of theory used to generate it. These computational methods can be validated by benchmarking against higher levels of theory and comparison of the rate constants and KIEs to experimental measurements. The calculations predicted that the KIE would decrease to ~1 for an E2PT process compared to the analogous E1PT process that exhibited a KIE of ~2.[22] This trend was subsequently verified experimentally, providing validation for the PCET theory.[22] This work highlighted the possibility that the KIE can be unity for a PCET reaction due to contributions from excited vibronic states with large overlaps between the reactant and product proton vibrational wavefunctions. This insight is relevant to experimentalists who often use the KIE as an indicator of proton transfer and presume that a KIE of unity implies the absence of proton transfer.

Using yet another computational strategy, nonequilibrium real-time dynamics simulations were performed to determine if the multiple proton transfer reactions are synchronous or asynchronous.[30] On the electrochemical timescale, the PCET mechanisms for up to four proton transfers (E4PT) appear to be concerted in that the infrared spectroelectrochemistry experiments observe either all protons on their donors or all protons on their acceptors with no partial proton transfers.[24] Moreover, DFT calculations of proton-coupled redox potentials indicated that the potentials computed with all protons transferred upon oxidation agree with the experimentally measured potentials.[24] Thus, from an electrochemical and thermodynamic perspective, these PCET processes are concerted with no thermodynamically stable intermediates. On the ultrafast timescale, however, nonequilibrium dynamics simulations revealed that these PCET reactions are asynchronous.[30] In these simulations, the BIP systems were equilibrated on the ground state, and the PCET reaction was induced by instantaneous oxidation (that is, electron removal). This situation corresponds to photochemically induced PCET, in which the electron transfers from the BIP molecule to a bound photosensitizer upon photoexcitation, as studied with TDDFT for fixed geometries of an E1PT BIP system.[31] Focusing on the real-time dynamics of an E2PT system, the first proton transfer occurred ~100 fs after electron transfer, and the second proton transfer occurred an average of ~600 fs after the first proton transfer (Figure 1C). These simulations highlight the fundamental principle that the identification of a PCET reaction as synchronous or asynchronous depends on the timescale considered.

A significant challenge for simulating these types of molecular PCET reactions is to perform nonequilibrium real-time dynamics with quantized protons and explicit solvent. The combination of QM/MM methods with path integral, wavepacket, or nuclear-electronic

Author Manuscript Author Manuscript Author Manuscript Author Manuscript

orbital (NEO)[32] methods to quantize the nuclei would be useful for these purposes. Simulations of electrochemically induced PCET reactions may also require an atomistic description of the electrode-solution interface, including electrolyte ions.

B. Photochemically induced PCET in triads

The anthracene-phenol-pyridine triads are also related to the tyrosine-histidine pair of photosystem II, where phenol represents tyrosine and pyridine represents histidine. As for the BIP molecules, understanding the fundamental PCET mechanism in these model systems is expected to provide insights into photosynthesis and other biological processes that rely on the oxidation of tyrosine. In these triads, photoexcitation of a local excited state (LES) of anthracene induces two PCET reactions (Figure 2).[33] The first PCET reaction consists of electron transfer from phenol to anthracene and proton transfer from phenol to pyridine, generating the charge separated state (CSS). The second PCET reaction is the charge recombination reaction leading back to the ground state. A series of triads with different substituents associated with a range of driving forces, defined as the negative of the PCET reaction free energy $-\Delta G^{o}$, was investigated both experimentally and computationally.

These triads served as the basis for illustrating inverted region behavior for a PCET reaction. In the inverted region, the more thermodynamically favorable reaction is slower. Marcus theory for electron transfer predicted that certain electron transfer reactions would exhibit inverted region behavior[15, 34] due to the exponential dependence of the rate constant on the free energy barrier, $\Delta G^{\ddagger} = \frac{\left(\Delta G^{o} + \lambda\right)^{2}}{(4\lambda)}$, where $-\Delta G^{o}$ is the driving force and λ is the reorganization energy. When $-\Delta G^{o} = \lambda$, the free energy barrier is zero (that is, the reaction is activationless), and as the driving force increases such that $-\Delta G^{o} > \lambda$, the free energy barrier increases and therefore the rate constant decreases. This inverted region behavior was confirmed experimentally for electron transfer.[35] For some PCET reactions, the inverted region may not be observable[36] because contributions from excited product vibronic states could lead to a plateau in the rate constant, where one state is always nearly activationless, as the driving force increases within the experimentally accessible range. For three of the triads, however, the inverted region was observed experimentally for the charge recombination step (Figure 2B).[33] According to the vibronically nonadiabatic PCET theory, the inverted region for PCET may be observed if the relevant excited product vibronic states do not contribute to the rate constant due to prohibitively small overlap arising from phase cancellation for oscillatory excited proton vibrational wavefunctions.[33, 37] This criterion was found to be satisfied when the analytical nonadiabatic PCET theory was applied to the three triads exhibiting inverted region behavior. Moreover, the KIE for the charge recombination step was calculated and experimentally observed to be unity,[33] similar to the E2PT BIP system for the same basic reason.

In an effort to explain why only three of the triads studied exhibited inverted region behavior, the nonequilibrium excited state dynamics for the initial PCET reaction following photoexcitation was simulated using TDDFT (Figure 2A).[38] The system was equilibrated in the ground state and then instantaneously placed in the LES, which was the S_1 state,

Author Manuscript Author Manuscript Author Manuscript Author Manuscript

followed by adiabatic excited state dynamics on the S_1 state. For the triads that exhibited inverted region behavior, the S_1 state changed character to the CSS, indicating electron transfer from phenol to anthracene and proton transfer from phenol to pyridine. For the other triads, however, the S_1 state changed character to a state characterized as local electron-proton transfer (LEPT), corresponding to electron and proton transfer from phenol to pyridine, namely excited state proton transfer within the phenol-pyridine pair. This behavior was also observed with higher-level multireference wavefunction calculations, such as CASSCF+NEVPT2.[39]

Recently, this prediction of the LEPT state was verified experimentally in a butyronitrile glass at 77 K.[8] In these experiments, photoexcitation to the LES resulted in fluorescence from the LEPT state, which would be quenched at room temperature due to a twist between the phenol and pyridine. The combined experimental and computational analysis led to the discovery of the proton-coupled energy transfer (PCEnT) mechanism. This mechanism entails electronic energy transfer from anthracene to the phenol-pyridine fragment coupled to proton tunneling without charge transfer to anthracene. This system serves as an example of how computational studies can make a prediction, such as the LES to LEPT mechanism in these triads, that is subsequently validated experimentally to reveal a new type of fundamental mechanism.

In addition to computational challenges such as quantizing the transferring protons and including explicit solvent, simulating photoinduced molecular PCET reactions requires an accurate description of excited state potential energy surfaces. Moreover, the nuclei are expected to move on multiple surfaces, necessitating the use of nonadiabatic dynamics methods.[40, 41]

III. PCET in enzymes

PCET in enzymatic systems is often activated by the binding of substrate or an effector, as well as thermal fluctuations of the solvated protein system. This section will discuss an example of a single PCET reaction in soybean lipoxygenase (SLO) and an example of a series of six coupled PCET reactions in ribonucleotide reductase (RNR). Although similar computational methods can be applied to the PCET reactions in both enzymes, the description of multiple coupled PCET reactions is more challenging and requires kinetic modeling techniques to describe the overall multi-PCET process. Understanding PCET in enzymes is important for controlling biochemical processes as well as for guiding protein engineering and drug design.

A. PCET in soybean lipoxygenase

SLO catalyzes the net hydrogen atom transfer from the linoleic acid substrate to the iron cofactor. In this rate-limiting PCET reaction,[42] the electron transfers from the π-backbone of the substrate to the iron, while the proton transfers from the C11 carbon of the substrate to the oxygen of the hydroxyl ligand (Figure 3A). A concerted mechanism is supported by thermodynamic considerations because single electron and single proton transfer are highly endoergic, whereas the concerted process is exoergic, so the reaction will be concerted to avoid high-energy intermediates. SLO has served as a prototype for hydrogen tunneling in

Author Manuscript Author Manuscript Author Manuscript Author Manuscript

enzymes because of its experimentally observed KIE of ~80 at room temperature for the wild-type enzyme[26, 27] and ~700 for the L546A/L754A double mutant.[28] These remarkably high KIEs are hallmarks of hydrogen tunneling and nonadiabaticity.

A variety of theoretical methods have been applied to SLO.[27, 43–48] Some of these studies performed atomistic MD simulations including hydrogen tunneling with methods such as path integrals[44] or variational transition state theory with multidimensional tunneling contributions.[45] Initial applications of vibronically nonadiabatic PCET theory to SLO[43, 46] used DFT calculations on small model systems of the active site and classical MD of the entire solvated enzyme system to compute the input quantities to the analytical rate constant expression given in Eq. (1). According to this PCET theory, the KIE associated with each term in the double summation is proportional to the ratio of the square of the overlap integrals for hydrogen and deuterium (Figure 3B). This ratio increases as the overlap decreases, that is, as the proton donor-acceptor distance increases. Because the proton transfers from a carbon to an oxygen atom, corresponding to a weak CH – – – O hydrogen bond, the proton donor-acceptor C–O distance is relatively large, leading to a high ratio of the hydrogen and deuterium overlap integrals and thus a large KIE. From a physical perspective, a substantial difference between the hydrogen and deuterium overlap integrals corresponds to a large difference in the hydrogen and deuterium tunneling probabilities and hence a high KIE. The double mutant was proposed to have an even longer C–O distance to explain its even higher KIE.[28]

Subsequently, QM/MM free energy simulations provided more detailed mechanistic information on the atomic level.[48] The substrate and cofactor were treated with DFT, and the remainder of the solvated protein system was treated with molecular mechanics. The finite temperature string method with umbrella sampling[49] was used to compute the free energy as a function of the C–O, C–H, and O–H distances for both the wild-type and double mutant SLO systems (Figure 3C).[48] The resulting free energy profiles confirmed that the double mutant has a larger equilibrium C–O distance than the wild-type enzyme. Moreover, these simulations, as well as classical MD simulations,[50] also showed that the double mutant has a larger cavity for substrate binding because the two leucine residues bracketing the proton donor, C11, on the substrate were mutated to smaller alanine residues (Figure 3A). The larger substrate binding cavity leads to a less optimal orientation of the CH – – – O interface, a smaller overlap between the vibrational wavefunctions, and a larger ratio of the hydrogen and deuterium overlap integrals. The greater difference in hydrogen and deuterium tunneling probabilities is responsible for the colossal KIE of ~700 observed for the double mutant. This example illustrates the importance of combining atomistic classical MD and QM/MM free energy simulations with analytical theories to explain PCET mechanisms in enzymatic systems.

Given the importance of hydrogen tunneling and conformational sampling for this enzyme, simulations must treat the transferring proton quantum mechanically as well as include the solvated protein environment. An additional challenge arises because this PCET reaction is vibronically and electronically nonadiabatic,[51] and therefore simulations must include the effects of excited vibronic states. To address this challenge, nonadiabatic dynamics methods can be implemented for vibronic surfaces beyond the Born-Oppenheimer

Author Manuscript Author Manuscript Author Manuscript Author Manuscript

approximation,[52, 53] although extending such approaches to proteins will require additional methodological developments, such as combining the NEO method[32, 54] with QM/MM approaches. Similar approaches could be applied to other enzymes catalyzing nonadiabatic PCET, such as cytochrome bc_1.[19, 55]

B. PCET in ribonucleotide reductase

RNR catalyzes the conversion of ribonucleotides to deoxyribonucleotides and is essential for DNA synthesis and repair in all living organisms.[56, 57] The prototypical RNR that has been studied extensively is *E. coli*, a member of the same RNR class as human and mouse. In this enzyme, catalysis requires radical transfer over ~32 Å through a series of six PCET steps between amino acids (Figure 4A).[57, 58] Understanding this complex PCET pathway, including the fundamental mechanisms of the individual steps and how they are coupled to each other and to protein conformational motions, has biochemical and potentially pharmacological implications. Individual PCET reactions modeled from fragments of the RNR protein have been studied using various quantum chemistry methods.[59–62] Recently, a cryo-EM structure of *E. coli* RNR was solved, revealing the complete ordered PCET pathway.[63] This structure enabled computational studies of the full protein system with a combination of classical MD, QM/MM free energy simulations, and kinetic modeling.

Classical MD simulations based on the cryo-EM structure of RNR provided insights into protein conformational motions and hydrogen-bonding interactions.[64] These simulations illustrated that water hydrogen bonds to several tyrosine residues along the PCET pathway, including Y356, Y731, and Y730. Moreover, free energy simulations showed that the interfacial residue Y731 is able to sample two conformations: a conformation where Y731 is stacked with Y730 and a conformation where Y731 is flipped out pointing toward the interface. Evidence for these two conformations had also been obtained experimentally.[65, 66]

QM/MM free energy simulations using the finite temperature string method with umbrella sampling clarified the mechanisms of two individual PCET steps along the radical transfer pathway. Such free energy simulations suggested that PCET between Y730 and Y731 is mediated by E623 through a proton relay mechanism involving double proton transfer with the proton residing temporarily on E623.[67] Analogous free energy simulations of PCET between Y730 and C439 highlighted the role of hydrogen-bonding interactions between Y730 and either E623 or water.[68] These QM/MM free energy simulations illustrate that the conformational motions and electrostatic interactions of the key residues as well as nearby water molecules impact both the thermodynamics and kinetics of the individual PCET steps.

In addition to atomistic simulations of the individual PCET steps, a kinetic model was designed to describe the reversible radical transfer process along the PCET pathway in RNR (Figure 4B).[69] Such kinetic models have been used to elucidate related processes in other biological systems.[70, 71] The kinetic model for RNR was based on experimental studies of photoRNR systems,[72, 73] which contain a photosensitizer ligated to a residue adjacent to Y356. Illumination of the photosensitizer with light causes the photosensitizer to oxidize Y356, thereby injecting a radical into the PCET pathway. Although the radical lifetime of Y356 was monitored experimentally, the kinetics of the individual steps could not be resolved. The mathematical kinetic model filled this gap by illustrating the time evolution

Author Manuscript Author Manuscript Author Manuscript Author Manuscript

of radical transport along the PCET pathway.[69] It also identified the rate constants that exert the greatest impact on the overall timescale of radical transport. Ranges for most of the individual rate constants in the kinetic model were determined from experimental measurements and atomistic QM/MM free energy simulations. This example highlights the importance of combining atomistic simulations and kinetic models to understand the coupling among multiple PCET reactions and protein conformational motions in complex biological systems (Figure 4C).

The real-time dynamics simulation of the entire radical transfer pathway, encompassing the six PCET reactions as well as both slow and fast conformational motions in RNR, is especially challenging. For such a large and complex system, coarse-graining[74] portions of the enzyme may be warranted, and multiscale simulation methods would be necessary.

IV. PCET in photoreceptors

Light-activated photoreceptor proteins are important for long-range signaling in cells and have applications to optogenetics. The Slr1694 blue-light using flavin (BLUF) photoreceptor protein undergoes forward and reverse PCET during its photocycle.[75–77] Photoexcitation to a local excited (LE) state of the flavin induces electron transfer from Tyr8 to the flavin, followed by double proton transfer from Tyr8 to the flavin via the intervening Gln50, generating the neutral flavin radical. A reverse PCET reaction returns the flavin and Tyr8 to their original oxidation and protonation states. At this point of the photocycle, the system is in a thermally excited state called the light-adapted state, which is capable of sending a long-range signal to cause a cellular response. Understanding the mechanism of this photocycle and characterizing the light-adapted state are important for engineering photoreceptors with specified properties and signaling capabilities.

A wide range of computational methods have been applied to BLUF photoreceptors.[9, 78–85] Focusing on the Slr1694 BLUF photoreceptor, free energy simulations have identified the thermodynamically stable configurations of the active site. Specifically, these simulations probed the location and orientation of Trp91 and the orientation of Gln50, which can form a proton relay between Tyr8 and the flavin.[84] Moreover, multireference wavefunction calculations, such as CASSCF+NEVPT2, of the two-dimensional ground and excited state proton potential energy surfaces have indicated that the double proton transfer reaction occurs sequentially after the initial electron transfer from Tyr8 to flavin.[85] These multireference calculations also provided a benchmark for the TDDFT method used in subsequent on-the-fly MD simulations.[86]

To simulate the real-time dynamics of the BLUF photocycle, the system was equilibrated in the ground state and instantaneously photoexcited to the S_1 LE state.[9] Nonequilibrium excited state MD trajectories propagated on the S_1 state confirmed that double proton transfer follows the initial electron transfer and suggested that Gln50 subsequently rotates, providing an alternative route for reverse PCET from the flavin back to Tyr8 (Figure 5). On the basis of these simulations, the light-adapted state was hypothesized to be characterized by the rotated imidic acid tautomer of Gln50.[9] Similar proposals for other BLUF photoreceptors had been made previously in the literature based on experimental data[81, 87]

Author Manuscript Author Manuscript Author Manuscript Author Manuscript

or static calculations.[78–81] This hypothesis was tested for the Slr1694 BLUF photoreceptor by calculating the electronic absorption spectrum of the flavin using TDDFT and the infrared vibrational stretch of the flavin C4 = O using an anharmonic grid-based approach. These spectra were averaged over many conformations of the dark- and light-adapted states procured from the real-time dynamics simulations.[9] The conformationally averaged electronic and vibrational spectra exhibited red-shifts in agreement with experimental measurements[88] on the light-adapted state. This example showcases the importance of utilizing a variety of methods, including QM/MM free energy simulations, multireference calculations, and nonequilibrium excited state dynamics, for investigating photoreceptor proteins.

The challenges encountered for simulating PCET in photoreceptors are similar to those discussed above for simulating photoinduced PCET in solution except the systems are larger and the photocycles are often more complex. In addition, an accurate description of the diradical state in this BLUF photoreceptor requires multireference wavefunction methods, which are computationally expensive, particularly for nonadiabatic dynamics with quantized nuclei. The relatively long timescale of the BLUF photocycle creates an additional challenge. Approaches such as coarse-grained modeling[89] and accelerated molecular dynamics,[90] as well as kinetic modeling,[69] could be used to address these challenges.

V. Concluding remarks and future prospects

The most effective strategy for exploring PCET reactions is to employ a wide range of different types of computational methods, spanning analytical theories, atomistic simulations, spectroscopic simulations, and kinetic modeling. The input quantities to the analytical PCET theories, such as the driving forces and the proton potential energy surfaces, are often computed with DFT. Moreover, the QM region in QM/MM free energy simulations is also often treated with DFT for computational efficiency. Benchmarking various DFT exchange-correlation functionals against high-level multireference wavefunction calculations can guide the choice of functional for each system studied.[39, 67, 86] Comparing computed structural, kinetic, and spectroscopic data to experimental measurements,[9, 22] as well as providing predictions for experimental verification,[22] is another important part of this strategy.

In addition, the development of novel computational approaches that capture electronic and nuclear quantum effects, non-Born-Oppenheimer effects, and conformational motions on a wide range of length and time scales is essential for further progress. For example, methods that enable the real-time simulation of nuclear-electronic quantum dynamics beyond the Born-Oppenheimer approximation[52, 53] are directly applicable to PCET reactions. These NEO methods[54] will enable MD simulations in which the electrons and transferring proton(s) are treated quantum mechanically on the same level, thereby inherently incorporating zero-point energy, nuclear delocalization, and hydrogen tunneling associated with the quantized protons. Hybrid approaches that incorporate complex environments, such as heterogeneous solutions, proteins, and interfaces, open up more opportunities for the simulation of chemical and biological processes. For example, QM/QM methods with

Author Manuscript Author Manuscript Author Manuscript Author Manuscript

two different levels of quantum mechanics or QM/QM/MM methods that also include a molecular mechanical part can be combined with dielectric continuum models to expand the size of the systems studied, treating the most important part of the system at the highest level and the least important environmental part of the system at the lowest level. An important future direction is to treat one of the QM levels with the NEO method, thereby including the nuclear quantum effects of the transferring protons for complex condensed phase systems.

Machine learning (ML)[30, 91–94] is another tool that is expected to expand the capabilities in this field. In particular, ML could provide more accurate potential energy surfaces at a lower computational cost. This ML strategy has been demonstrated for simulations of liquid water with potential energy surfaces at coupled cluster singles, doubles, and perturbative triples accuracy including nuclear quantum effects via path integrals.[95] The main challenge of such ML strategies is that they require computationally intensive training for each type of system studied. In addition, ML can also be used to compute the proton vibrational wavefunctions and energy levels[94] for input into analytical PCET rate constant expressions. However, the training procedure for molecular PCET systems with multiple protons will be computationally expensive. Combining all of these computational strategies while maintaining a strong connection to experiments will continue to reveal the fundamental principles governing the coupled motions of electrons and protons in chemically and biologically significant processes.

Acknowledgments

The writing of this Perspective was funded by the National Institutes of Health grant number R35 GM139449 and the Air Force Office of Scientific Research under AFOSR Award No. FA9550-18-1-0134. The author thanks the following group members for their contributions to some of the previously published work discussed herein and assistance with the figures: M. T. Huynh, J. J. Goings, M. Secor, Z. K. Goldsmith, E. R. Sayfutyarova, Z. Tao, A. V. Soudackov, P. Li, C. R. Reinhardt, J. Zhong, and D. Konstantinovsky. We are also grateful to our experimental collaborators in previously published work: T. A. Moore, A. L. Moore, J. M. Mayer, L. Hammarström, J. P. Klinman, J. Stubbe, and C. L. Drennan.

References

1. Huynh MHV & Meyer TJ Proton-coupled electron transfer. Chem. Rev 107, 5004–5064 (2007). [PubMed: 17999556]
2. Warren JJ, Tronic TA & Mayer JM Thermochemistry of proton-coupled electron transfer reagents and its implications. Chem. Rev 110, 6961–7001 (2010). [PubMed: 20925411]
3. Hammes-Schiffer S. & Stuchebrukhov AA Theory of coupled electron and proton transfer reactions. Chem. Rev 110, 6939–6960 (2010). [PubMed: 21049940]
4. Tyburski R, Liu T, Glover SD & Hammarström L. Proton-coupled electron transfer guidelines, fair and square. J. Am. Chem. Soc 143, 560–576 (2021). [PubMed: 33405896]
5. Warburton RE, Soudackov AV & Hammes-Schiffer S. Theoretical modeling of electrochemical proton-coupled electron transfer. Chem. Rev 122, 10599–10650 (2022). [PubMed: 35230812]
6. Gross EKU & Kohn W. Time-dependent density-functional theory. Adv. Quantum Chem 21, 255–291 (1990).
7. Lischka H, Nachtigallova D, Aquino AJ, Szalay PG, Plasser F, Machado FB & Barbatti M. Multireference approaches for excited states of molecules. Chem. Rev 118, 7293–7361 (2018). [PubMed: 30040389]
8. Pettersson Rimgard B, Tao Z, Parada GA, Cotter LF, Hammes-Schiffer S, Mayer JM & Hammarström L. Proton-coupled energy transfer in molecular triads. Science 377, 742–747 (2022). [PubMed: 35862490]

Author Manuscript Author Manuscript Author Manuscript Author Manuscript

9. Goings JJ, Li P, Zhu Q. & Hammes-Schiffer S. Formation of an unusual glutamine tautomer in a blue light using flavin photocycle characterizes the light-adapted state. Proc. Natl. Acad. Sci. U.S.A 117, 26626–26632 (2020). [PubMed: 33037153]
10. Li X, Tully JC, Schlegel HB & Frisch MJ Ab initio ehrenfest dynamics. J. Chem. Phys 123, 084106 (2005). [PubMed: 16164281]
11. Tully JC Molecular dynamics with electronic transitions. J. Chem. Phys 93, 1061–1071 (1990).
12. Soudackov A. & Hammes-Schiffer S. Multistate continuum theory for multiple charge transfer reactions in solution. J. Chem. Phys 111, 4672–4687 (1999).
13. Soudackov A. & Hammes-Schiffer S. Derivation of rate expressions for nonadiabatic proton-coupled electron transfer reactions in solution. J. Chem. Phys 113, 2385–2396 (2000).
14. Hammes-Schiffer S. & Soudackov AV Proton-coupled electron transfer in solution, proteins, and electrochemistry. J. Phys. Chem. B 112, 14108–14123 (2008). [PubMed: 18842015]
15. Marcus RA & Sutin N. Electron transfers in chemistry and biology. Biochim. Biophys. Acta 811, 265–322 (1985).
16. Stuchebrukhov AA Electron transfer reactions coupled to proton translocation. Cytochrome oxidase, proton pumps, and biological energy transduction. J. Theor. Comput. Chem 2, 91–118 (2003).
17. Klein JE & Knizia G. cPCET versus HAT: A direct theoretical method for distinguishing x–h bond-activation mechanisms. Angew. Chem. Int. Ed 57, 11913–11917 (2018).
18. Gaggioli CA, Sauer J. & Gagliardi L. Hydrogen atom or proton coupled electron transfer? C–h bond activation by transition-metal oxides. J. Am. Chem. Soc 141, 14603–14611 (2019). [PubMed: 31432676]
19. Camilo SR, Curtolo F, Galassi VV & Arantes GM Tunneling and nonadiabatic effects on a proton-coupled electron transfer model for the q o site in cytochrome bc 1. J. Chem. Inf. Model 61, 1840–1849 (2021). [PubMed: 33793213]
20. Tommos C. & Babcock GT Proton and hydrogen currents in photosynthetic water oxidation. Biochim. Biophys. Acta 1458, 199–219 (2000). [PubMed: 10812034]
21. Hammarström L. & Styring S. Proton-coupled electron transfer of tyrosines in photosystem II and model systems for artificial photosynthesis: The role of a redox-active link between catalyst and photosensitizer. Energy Environ. Sci 4, 2379–2388 (2011).
22. Huynh MT, et al. Concerted one-electron two-proton transfer processes in models inspired by the tyr-his couple of photosystem II. ACS Cent. Sci 3, 372–380 (2017). [PubMed: 28573198]
23. Odella E, et al. Controlling proton-coupled electron transfer in bioinspired artificial photosynthetic relays. J. Am. Chem. Soc 140, 15450–15460 (2018). [PubMed: 30379075]
24. Odella E, et al. Proton-coupled electron transfer drives long-range proton translocation in bioinspired systems. J. Am. Chem. Soc 141, 14057–14061 (2019). [PubMed: 31390197]
25. Odella E, et al. Managing the redox potential of PCET in grotthuss-type proton wires. J. Am. Chem. Soc 144, 15672–15679 (2022). [PubMed: 35993888]
26. Rickert KW & Klinman JP Nature of hydrogen transfer in soybean lipoxygenase 1: Separation of primary and secondary isotope effects. Biochemistry 38, 12218–12228 (1999). [PubMed: 10493789]
27. Knapp MJ, Rickert KW & Klinman JP Temperature dependent isotope effects in soybean lipoxygenase-1: Correlating hydrogen tunneling with protein dynamics. J. Am. Chem. Soc 124, 3865–3874 (2002). [PubMed: 11942823]
28. Hu S, et al. Extremely elevated room-temperature kinetic isotope effects quantify the critical role of barrier width in enzymatic O–H activation. J. Am. Chem. Soc 136, 8157–8160 (2014). [PubMed: 24884374]
29. Auer B, Fernandez LE & Hammes-Schiffer S. Theoretical analysis of proton relays in electrochemical proton-coupled electron transfer. J. Am. Chem. Soc 133, 8282–8292 (2011). [PubMed: 21524104]
30. Goings JJ & Hammes-Schiffer S. Nonequilibrium dynamics of proton-coupled electron transfer in proton wires: Concerted but asynchronous mechanisms. ACS Cent. Sci 6, 1594–1601 (2020). [PubMed: 32999935]

Author Manuscript Author Manuscript Author Manuscript Author Manuscript

31. Yoneda Y, et al. Electron–nuclear dynamics accompanying proton-coupled electron transfer. J. Am. Chem. Soc 143, 3104–3112 (2021). [PubMed: 33601880]
32. Tao Z, Yu Q, Roy S. & Hammes-Schiffer S. Direct dynamics with nuclear–electronic orbital density functional theory. Acc. Chem. Res 54, 4131–4141 (2021). [PubMed: 34726895]
33. Parada GA, et al. Concerted proton-electron transfer reactions in the Marcus inverted region. Science 364, 471–475 (2019). [PubMed: 30975771]
34. Marcus RA Exchange reactions and electron transfer reactions including isotopic exchange. Theory of oxidation-reduction reactions involving electron transfer. Part 4.—a statistical-mechanical basis for treating contributions from solvent, ligands, and inert salt. Discuss. Faraday Soc 29, 21–31 (1960).
35. Closs GL & Miller JR Intramolecular long-distance electron transfer in organic molecules. Science 240, 440–447 (1988). [PubMed: 17784065]
36. Edwards SJ, Soudackov AV & Hammes-Schiffer S. Driving force dependence of rates for nonadiabatic proton and proton-coupled electron transfer: Conditions for inverted region behavior. J. Phys. Chem. B 113, 14545–14548 (2009). [PubMed: 19795899]
37. Goldsmith ZK, Soudackov AV & Hammes-Schiffer S. Theoretical analysis of the inverted region in photoinduced proton-coupled electron transfer. Faraday Discuss., (2019).
38. Sayfutyarova ER & Hammes-Schiffer S. Excited state molecular dynamics of photoinduced proton-coupled electron transfer in anthracene–phenol–pyridine triads. J. Phys. Chem. Lett 11, 7109–7115 (2020). [PubMed: 32787327]
39. Sayfutyarova ER & Hammes-Schiffer S. Substituent effects on photochemistry of anthracene-phenol-pyridine triads revealed by multireference calculations. J. Am. Chem. Soc 142, 487–494 (2020). [PubMed: 31846322]
40. Curchod BFE & Martínez TJ Ab initio nonadiabatic quantum molecular dynamics. Chem. Rev 118, 3305–3336 (2018). [PubMed: 29465231]
41. Crespo-Otero R. & Barbatti M. Recent advances and perspectives on nonadiabatic mixed quantum–classical dynamics. Chem. Rev 118, 7026–7068 (2018). [PubMed: 29767966]
42. Glickman MH & Klinman JP Nature of rate-limiting steps in the soybean lipoxygenase-1 reaction. Biochemistry 34, 14077–14092 (1995). [PubMed: 7578005]
43. Hatcher E, Soudackov AV & Hammes-Schiffer S. Proton-coupled electron transfer in soybean lipoxygenase. J. Am. Chem. Soc 126, 5763–5775 (2004). [PubMed: 15125669]
44. Olsson MHM, Siegbahn PEM & Warshel A. Simulations of the large kinetic isotope effect and the temperature dependence of the hydrogen atom transfer in lipoxygenase J. Am. Chem. Soc 126, 2820–2828 (2004). [PubMed: 14995199]
45. Tejero I, Garcia-Viloca M, Gonzalez-Lafont A, Lluch JM & York DM Enzyme dynamics and tunneling enhanced by compression in the hydrogen abstraction catalyzed by soybean lipoxygenase-1. J. Phys. Chem. B 110, 24708–24719 (2006). [PubMed: 17134234]
46. Hatcher E, Soudackov AV & Hammes-Schiffer S. Proton-coupled electron transfer in soybean lipoxygenase: Dynamical behavior and temperature dependence of kinetic isotope effects. J. Am. Chem. Soc 129, 187–196 (2007). [PubMed: 17199298]
47. Salna B, Benabbas A, Russo D. & Champion PM Tunneling kinetics and nonadiabatic proton-coupled electron transfer in proteins: The effect of electric fields and anharmonic donor–acceptor interactions. J. Phys. Chem. B 121, 6869–6881 (2017). [PubMed: 28628313]
48. Li P, Soudackov AV & Hammes-Schiffer S. Fundamental insights into proton-coupled electron transfer in soybean lipoxygenase from quantum mechanical/molecular mechanical free energy simulations. J. Am. Chem. Soc 140, 3068–3076 (2018). [PubMed: 29392938]
49. Rosta E, Nowotny M, Yang W. & Hummer G. Catalytic mechanism of rna backbone cleavage by ribonuclease h from quantum mechanics/molecular mechanics simulations. J. Am. Chem. Soc 133, 8934–8941 (2011). [PubMed: 21539371]
50. Li P, Soudackov AV & Hammes-Schiffer S. Impact of mutations on the binding pocket of soybean lipoxygenase: Implications for proton-coupled electron transfer. J. Phys. Chem. Lett 9, 6444–6449 (2018). [PubMed: 30359035]

Author Manuscript Author Manuscript Author Manuscript Author Manuscript

51. Soudackov AV & Hammes-Schiffer S. Probing nonadiabaticity in the proton-coupled electron transfer reaction catalyzed by soybean lipoxygenase. J. Phys. Chem. Lett 5, 3274–3278 (2014). [PubMed: 25258676]
52. Zhao L, Tao Z, Pavošević F, Wildman A, Hammes-Schiffer S. & Li X. Real-time time-dependent nuclear− electronic orbital approach: Dynamics beyond the born–oppenheimer approximation. J. Phys. Chem. Lett 11, 4052–4058 (2020). [PubMed: 32251589]
53. Zhao L, Wildman A, Pavošević F, Tully JC, Hammes-Schiffer S. & Li X. Excited state intramolecular proton transfer with nuclear-electronic orbital ehrenfest dynamics. J. Phys. Chem. Lett 12, 3497–3502 (2021). [PubMed: 33792317]
54. Hammes-Schiffer S. Nuclear–electronic orbital methods: Foundations and prospects. J. Chem. Phys 155, 030901 (2021). [PubMed: 34293877]
55. Barragan AM, Soudackov AV, Luthey-Schulten Z, Hammes-Schiffer S, Schulten K. & Solov'yov IA Theoretical description of the primary proton-coupled electron transfer reaction in the cytochrome bc 1 complex. J. Am. Chem. Soc 143, 715–723 (2021). [PubMed: 33397104]
56. Stubbe J, Nocera DG, Yee CS & Chang MCY Radical initiation in the class i ribonucleotide reductase: Long-range proton-coupled electron transfer? Chem. Rev 103, 2167–2202 (2003). [PubMed: 12797828]
57. Minnihan EC, Nocera DG & Stubbe J. Reversible, long-range radical transfer in E. coli class ia ribonucleotide reductase. Acc. Chem. Res 46, 2524–2535 (2013). [PubMed: 23730940]
58. Uhlin U. & Eklund H. Structure of ribonucleotide reductase protein r1. Nature 370, 533–539 (1994). [PubMed: 8052308]
59. Siegbahn PEM, Eriksson L, Himo F. & Pavlov M. Hydrogen atom transfer in ribonucleotide reductase (RNR). J. Phys. Chem. B 102, 10622–10629 (1998).
60. Kaila VR & Hummer G. Energetics of direct and water-mediated proton-coupled electron transfer. J. Am. Chem. Soc 133, 19040–19043 (2011). [PubMed: 21988482]
61. Argirevic T, Riplinger C, Stubbe J, Neese F. & Bennati M. Endor spectroscopy and DFT calculations: Evidence for the hydrogen-bond network within α2 in the PCET of E. coli ribonucleotide reductase. J. Am. Chem. Soc 134, 17661–17670 (2012). [PubMed: 23072506]
62. Chen X, et al. Water promoting electron hole transport between tyrosine and cysteine in proteins via a special mechanism: Double proton coupled electron transfer. J. Am. Chem. Soc 136, 4515–4524 (2014). [PubMed: 24601637]
63. Kang G, Taguchi AT, Stubbe J. & Drennan CL Structure of a trapped radical transfer pathway within a ribonucleotide reductase holocomplex. Science 368, 424–427 (2020). [PubMed: 32217749]
64. Reinhardt CR, Li P, Kang G, Stubbe J, Drennan CL & Hammes-Schiffer S. Conformational motions and water networks at the α/β interface in E. coli ribonucleotide reductase. J. Am. Chem. Soc 142, 13768–13778 (2020). [PubMed: 32631052]
65. Kasanmascheff M, Lee W, Nick TU, Stubbe J. & Bennati M. Radical transfer in E. coli ribonucleotide reductase: A nh2y731/r411a-α mutant unmasks a new conformation of the pathway residue 731. Chem. Sci 7, 2170–2178 (2016). [PubMed: 29899944]
66. Greene BL, Taguchi AT, Stubbe J. & Nocera DG Conformationally dynamic radical transfer within ribonucleotide reductase. J. Am. Chem. Soc 139, 16657–16665 (2017). [PubMed: 29037038]
67. Reinhardt CR, Sayfutyarova ER, Zhong J. & Hammes-Schiffer S. Glutamate mediates proton-coupled electron transfer between tyrosines 730 and 731 in escherichia coli ribonucleotide reductase. J. Am. Chem. Soc 143, 6054–6059 (2021). [PubMed: 33856807]
68. Zhong J, Reinhardt CR & Hammes-Schiffer S. Role of water in proton-coupled electron transfer between tyrosine and cysteine in ribonucleotide reductase. J. Am. Chem. Soc 144, 7208–7214 (2022). [PubMed: 35426309]
69. Reinhardt CR, Konstantinovsky D, Soudackov AV & Hammes-Schiffer S. Kinetic model for reversible radical transfer in ribonucleotide reductase. Proc. Natl. Acad. Sci. U.S.A 119, e2202022119 (2022). [PubMed: 35714287]
70. Yuly JL, Zhang P, Lubner CE, Peters JW & Beratan DN Universal free-energy landscape produces efficient and reversible electron bifurcation. Proc. Natl. Acad. Sci. U.S.A 117, 21045–21051 (2020). [PubMed: 32801212]

Author Manuscript Author Manuscript Author Manuscript Author Manuscript

71. van Wonderen JH, et al. Nanosecond heme-to-heme electron transfer rates in a multiheme cytochrome nanowire reported by a spectrally unique his/met-ligated heme. Proc. Natl. Acad. Sci. U.S.A 118, e2107939118 (2021). [PubMed: 34556577]
72. Olshansky L, Pizano AA, Wei Y, Stubbe J. & Nocera DG Kinetics of hydrogen atom abstraction from substrate by an active site thiyl radical in ribonucleotide reductase. J. Am. Chem. Soc 136, 16210–16216 (2014). [PubMed: 25353063]
73. Olshansky L, Stubbe J. & Nocera DG Charge-transfer dynamics at the α/β subunit interface of a photochemical ribonucleotide reductase. J. Am. Chem. Soc 138, 1196–1205 (2016). [PubMed: 26710997]
74. Saunders MG & Voth GA Coarse-graining methods for computational biology. Annu. Rev. Biophys 42, 73–93 (2013). [PubMed: 23451897]
75. Gauden M, van Stokkum IHM, Key JM, Luhrs DC, van Grondelle R, Hegemann P. & Kennis JTM Hydrogen-bond switching through a radical pair mechanism in a flavin-binding photoreceptor. Proc. Natl. Acad. Sci. U.S.A 103, 10895–10900 (2006). [PubMed: 16829579]
76. Kennis JTM & Mathes T. Molecular eyes: Proteins that transform light into biological information. Interface Focus 3, 20130005 (2013).
77. Mathes T, van Stokkum IH & Kennis J. Photoactivation mechanisms of flavin-binding photoreceptors revealed through ultrafast spectroscopy and global analysis methods. Methods Mol. Biol 1146, 401–442 (2014).
78. Sadeghian K, Bocola M. & Schutz M. A conclusive mechanism of the photoinduced reaction cascade in blue light using flavin photoreceptors. J. Am. Chem. Soc 130, 12501–12513 (2008). [PubMed: 18722438]
79. Domratcheva T, Grigorenko BL, Schlichting I. & Nemukhin AV Molecular models predict light-induced glutamine tautomerization in bluf photoreceptors. Biophys. J 94, 3872–3879 (2008). [PubMed: 18263659]
80. Khrenova MG, Nemukhin AV & Domratcheva T. Photoinduced electron transfer facilitates tautomerization of the conserved signaling glutamine side chain in bluf protein light sensors. J. Phys. Chem. B 117, 2369–2377 (2013). [PubMed: 23350608]
81. Domratcheva T, Hartmann E, Schlichting I. & Kottke T. Evidence for tautomerisation of glutamine in bluf blue light receptors by vibrational spectroscopy and computational chemistry. Sci. Rep 6, 22669 (2016). [PubMed: 26947391]
82. Goyal P. & Hammes-Schiffer S. Role of active site conformational changes in photocycle activation of the appa bluf photoreceptor. Proc. Natl. Acad. Sci. U.S.A 114, 1480–1485 (2017). [PubMed: 28137837]
83. Hashem S, Macaluso V, Nottoli M, Lipparini F, Cupellini L. & Mennucci B. From crystallographic data to the solution structure of photoreceptors: The case of the appa bluf domain. Chem. Sci 12, 13331–13342 (2021). [PubMed: 34777752]
84. Goings JJ, Reinhardt CR & Hammes-Schiffer S. Propensity for proton relay and electrostatic impact of protein reorganization in Slr1694 bluf photoreceptor. J. Am. Chem. Soc 140, 15241–15251 (2018). [PubMed: 30295026]
85. Sayfutyarova ER, Goings JJ & Hammes-Schiffer S. Electron-coupled double proton transfer in the Slr1694 bluf photoreceptor: A multireference electronic structure study. J. Phys. Chem. B 123, 439–447 (2018).
86. Goings JJ & Hammes-Schiffer S. Early photocycle of Slr1694 blue-light using flavin photoreceptor unraveled through adiabatic excited-state quantum mechanical/molecular mechanical dynamics. J. Am. Chem. Soc 141, 20470–20479 (2019). [PubMed: 31741389]
87. Stelling AL, Ronayne KL, Nappa J, Tonge PJ & Meech SR Ultrafast structural dynamics in bluf domains: Transient infrared spectroscopy of appa and its mutants. J. Am. Chem. Soc 129, 15556–15564 (2007). [PubMed: 18031038]
88. Masuda S, Hasegawa K, Ishii A. & Ono T. Light-induced structural changes in a putative blue-light receptor with a novel fad binding fold sensor of blue-light using fad (bluf); Slr1694 of synechocystis sp. Pcc6803. Biochemistry 43, 5304–5313 (2004). [PubMed: 15122896]
89. Kmiecik S, Gront D, Kolinski M, Wieteska L, Dawid AE & Kolinski A. Coarse-grained protein models and their applications. Chem. Rev 116, 7898–7936 (2016). [PubMed: 27333362]

Author Manuscript Author Manuscript Author Manuscript Author Manuscript

90. Tiwary P. & Walle A. v. d. A review of enhanced sampling approaches for accelerated molecular dynamics. Multiscale materials modeling for nanomechanics, 195–221 (2016).

91. Wang C-I, Braza MKE, Claudio GC, Nellas RB & Hsu C-P Machine learning for predicting electron transfer coupling. J. Phys. Chem. A 123, 7792–7802 (2019). [PubMed: 31429287]

92. Sauceda HE, Chmiela S, Poltavsky I, Müller K-R & Tkatchenko A. Molecular force fields with gradient-domain machine learning: Construction and application to dynamics of small molecules with coupled cluster forces. J. Chem. Phys 150, 114102 (2019). [PubMed: 30901990]

93. Brorsen KR Reproducing global potential energy surfaces with continuous-filter convolutional neural networks. J. Chem. Phys 150, 204104 (2019). [PubMed: 31153202]

94. Secor M, Soudackov AV & Hammes-Schiffer S. Artificial neural networks as mappings between proton potentials, wave functions, densities, and energy levels. J. Phys. Chem. Lett 12, 2206–2212 (2021). [PubMed: 33630595]

95. Daru J, Forbert H, Behler J. & Marx D. Coupled cluster molecular dynamics of condensed phase systems enabled by machine learning potentials: Liquid water benchmark. Phys. Rev. Lett 129, 226001 (2022). [PubMed: 36493459]

Author Manuscript Author Manuscript Author Manuscript Author Manuscript

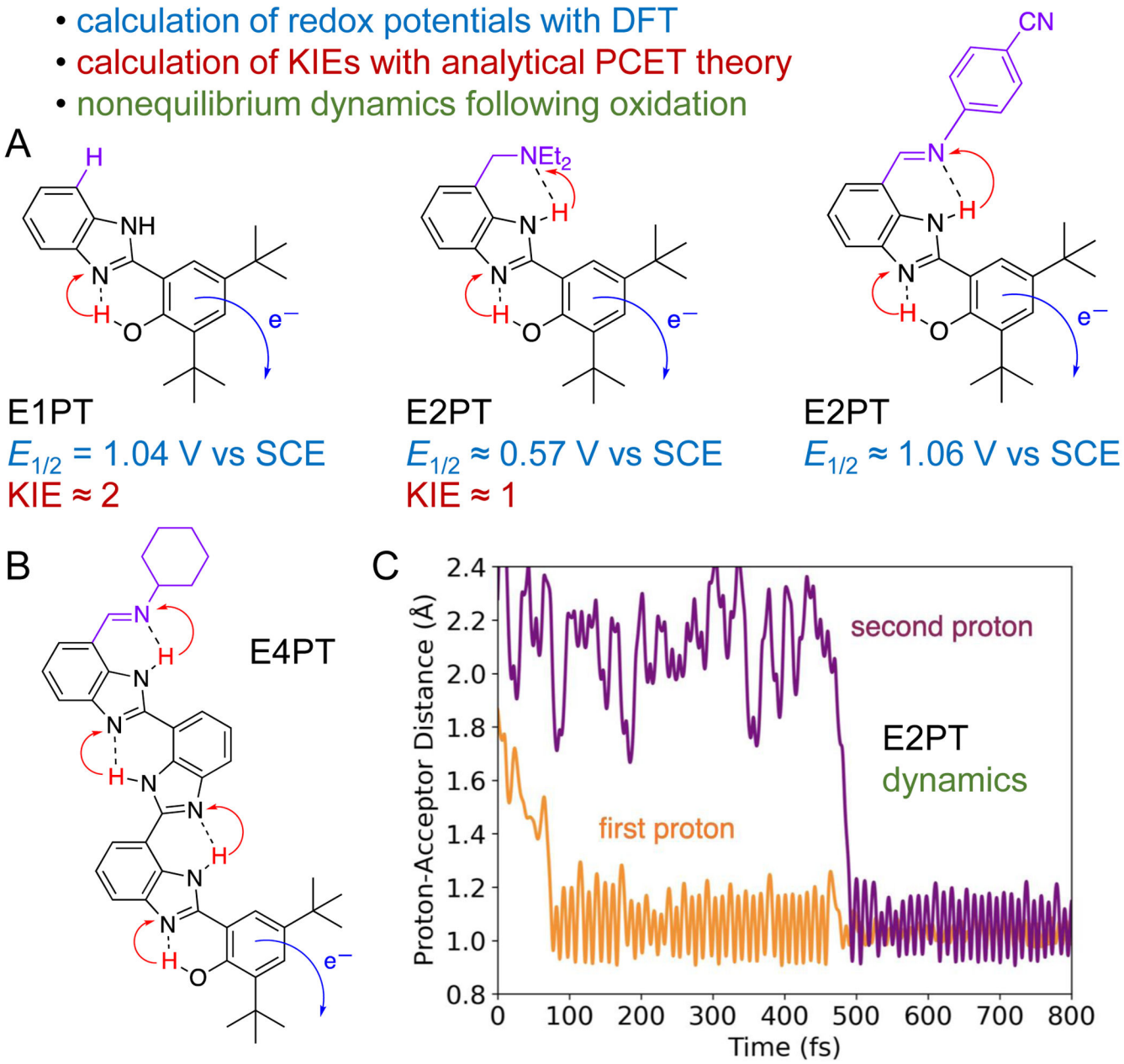

Figure 1:

Computationally guided design of BIP molecules. (A) Starting from E1PT (only one proton transferred), computation assisted in designing an E2PT system (two protons transferred), predicting the decrease in the proton-coupled redox potential $E_{1/2}$ and the KIE. The proton-coupled redox potentials $E_{1/2}$ given here were measured experimentally and agree well with the computed values. Further calculations assisted in designing an E2PT system with a higher redox potential of ~1 V vs SCE (saturated calomel electrode) necessary for artificial photosynthetic systems that split water. (B) Computation also assisted in designing an E4PT system that transports four protons over ~16 Å upon oxidation. (C) Nonequilibrium dynamics simulations showed that the two proton transfers are asynchronous for an E2PT

Author Manuscript Author Manuscript Author Manuscript Author Manuscript

system. The identification of a PCET reaction as synchronous or asynchronous depends on the timescale considered and, in this case, requires real-time dynamics simulations. The colors of the calculated quantities correspond to the methods used to calculate them. Part C adapted with permission from Ref. [30].

Author Manuscript
Author Manuscript
Author Manuscript
Author Manuscript

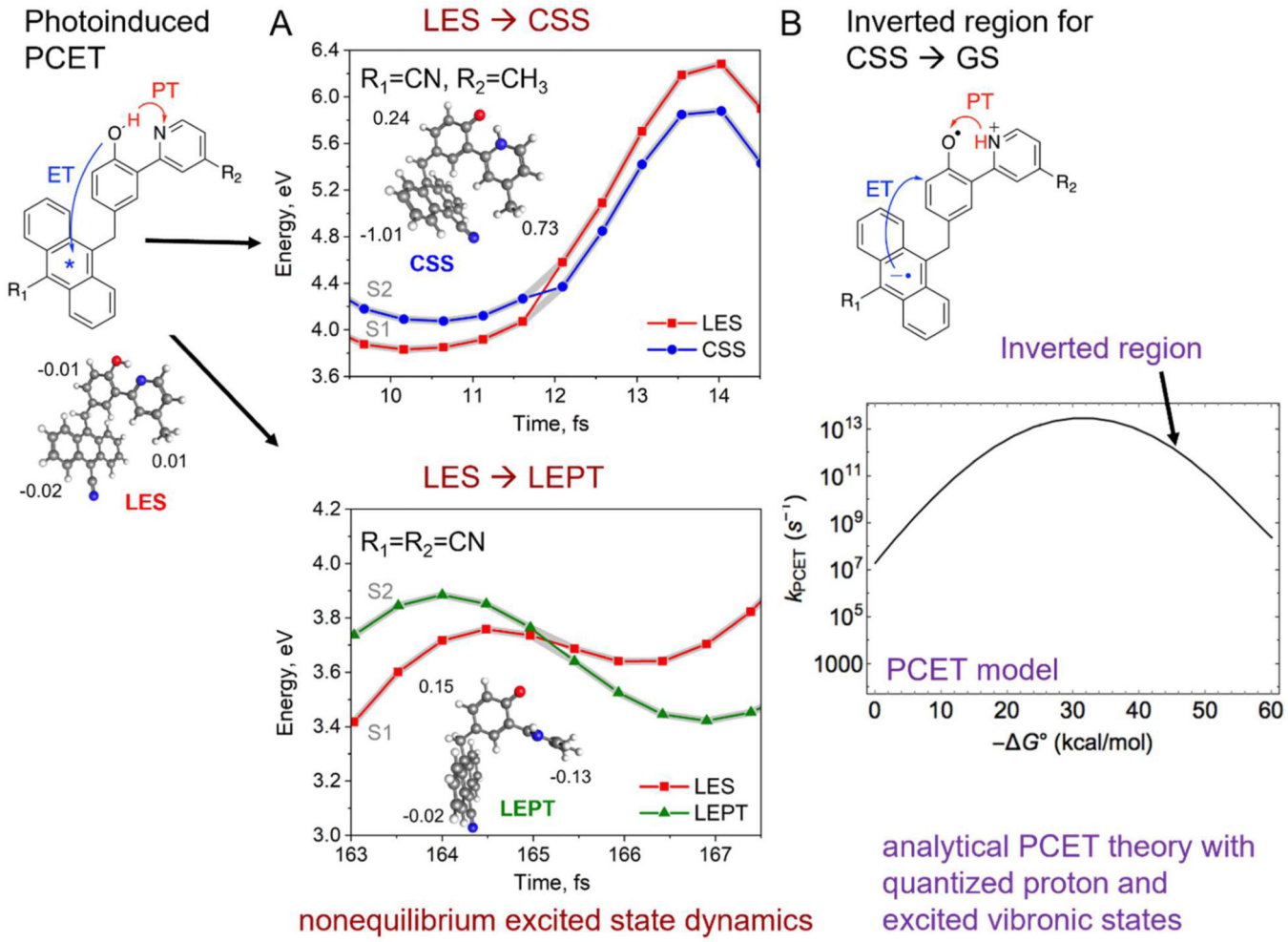

Figure 2:

Anthracene-phenol-pyridine triads that exhibit both PCET and PCEnT. Photoexcitation of the anthracene LES (local excited state, indicated by an asterisk in the molecule on the left) leads to the CSS (charge separated state) via PCET and then inverted region behavior upon charge recombination back to the GS (ground state) for some triads (horizontal arrow and top figures) but leads to the LEPT (local electron-proton transfer) state via PCEnT without charge transfer to anthracene or inverted region behavior for other triads (diagonal arrow and lowest plot). (A) Nonequilibrium, real-time dynamics trajectories in the S_1 state; the timescales and energy fluctuations are not comparable to experiment due to the initial conditions. The optimized structures of the relevant states are provided; the phenol-pyridine twisting in the LEPT state is impeded at 77 K. The partial charges on the anthracene, phenol, and pyridine fragments are also provided, showing that electron transfer to anthracene occurs only for the CSS. (B) The inverted region is depicted for a PCET model system for illustrative purposes. In the molecules, the atoms are carbon (gray), hydrogen (white), nitrogen (blue), and oxygen (red). The colors of the plot titles correspond to the computational methods used to generate them. The plots in part A were adapted with permission from Ref. [38], and the plot in part B was adapted with permission from Ref. [37].

Author Manuscript Author Manuscript Author Manuscript Author Manuscript

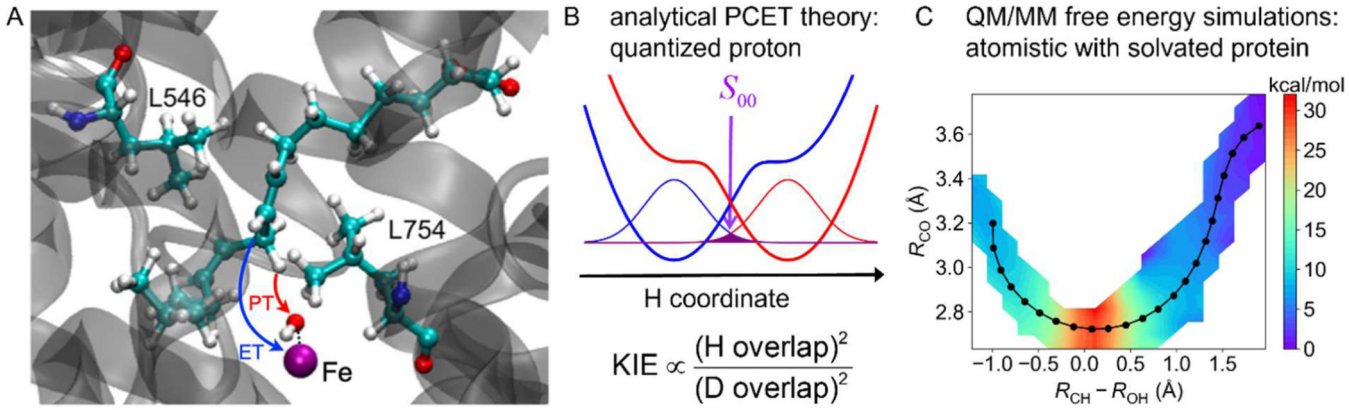

Figure 3:

PCET in soybean lipoxygenase. (A) The electron transfers from the **π**-backbone of the substrate to the iron, which is coordinated to other residues not shown, and the proton transfers from C11 of the substrate to the OH ligand. (B) Schematic of proton potential energy curves and corresponding proton vibrational wavefunctions for reactant (blue) and product (red) with overlap shown in purple. (c) Free energy surface as a function of the proton donor-acceptor distance R_{CO} and the proton transfer coordinate $R_{CH} - R_{OH}$ generated with the QM/MM finite temperature string method with umbrella sampling, where the minimum free energy path is shown in black. The high KIE of ~80 for the wild-type enzyme is explained by the dominant ground state hydrogen tunneling, which is associated with a relatively small overlap S_{00} between the reactant and product proton vibrational wavefunctions (purple shaded region in B) and a large ratio of the square of the H and D overlaps (equation in B). The two labeled leucine residues in A are mutated to alanine in the double mutant that exhibits a KIE of ~700. According to atomistic MD simulations, this mutation increases the size of the substrate binding cavity, leading to a less optimal orientation, larger equilibrium R_{CO}, smaller overlap S_{00}, larger ratio of H and D overlaps, and thus a larger KIE. The enzyme depiction and free energy surface were adapted with permission from Ref. [48].

Author Manuscript Author Manuscript Author Manuscript Author Manuscript

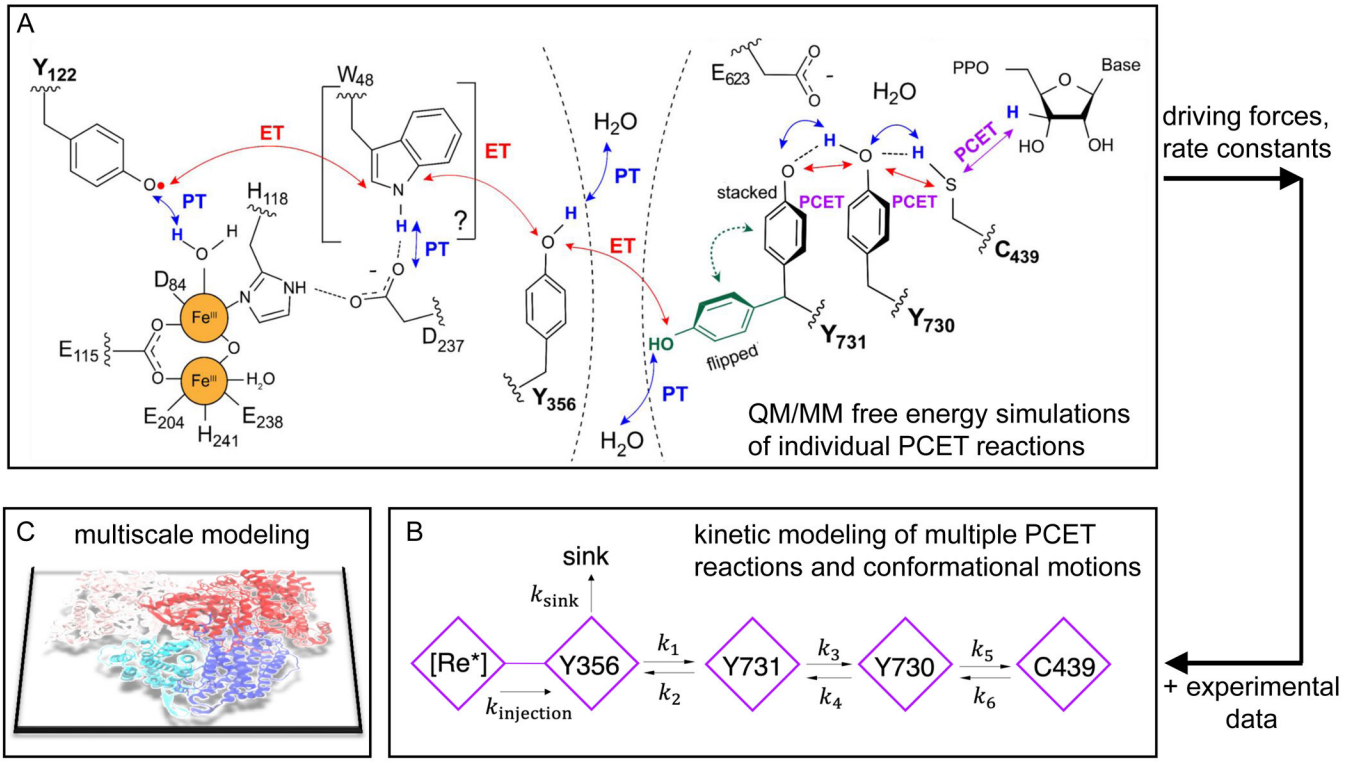

Figure 4:

PCET pathway in RNR and kinetic model to describe radical transfer along this pathway in a photoRNR with a Re photosensitizer ligated adjacent to Y356. (A) The PCET pathway is Y122 ↔ [W48] ↔ Y356 ↔ Y731 ↔ Y730 ↔ C439, shown in bold, where W48 is in square brackets because its participation is uncertain. Blue arrows show proton transfer (PT), red arrows show electron transfer (ET), and purple arrows show collinear PCET. MD simulations and experiments indicate that Y731 samples both the stacked and flipped conformations. QM/MM free energy simulations imply that E623 mediates PCET between Y731 and Y730 and that a water molecule interacts with Y730 when Y731 is in the flipped conformation. (B) The kinetic model includes radical injection from the photoexcited Re*, an off-pathway sink, radical transfer between pairs of residues along the pathway, and the conformational flipping/stacking motion of interfacial Y731. (C) Multiscale modeling of RNR (cryo-EM structure shown) requires the combination of atomistic simulations and kinetic modeling. The driving forces and rate constants serving as input to the kinetic model are estimated from a combination of QM/MM free energy simulations and experimental data, as indicated by the arrows pointing out of part A (output from QM/MM free energy simulations) and into part B (input to kinetic model). Parts A and B adapted with permission from Refs. [64] and [69], respectively.

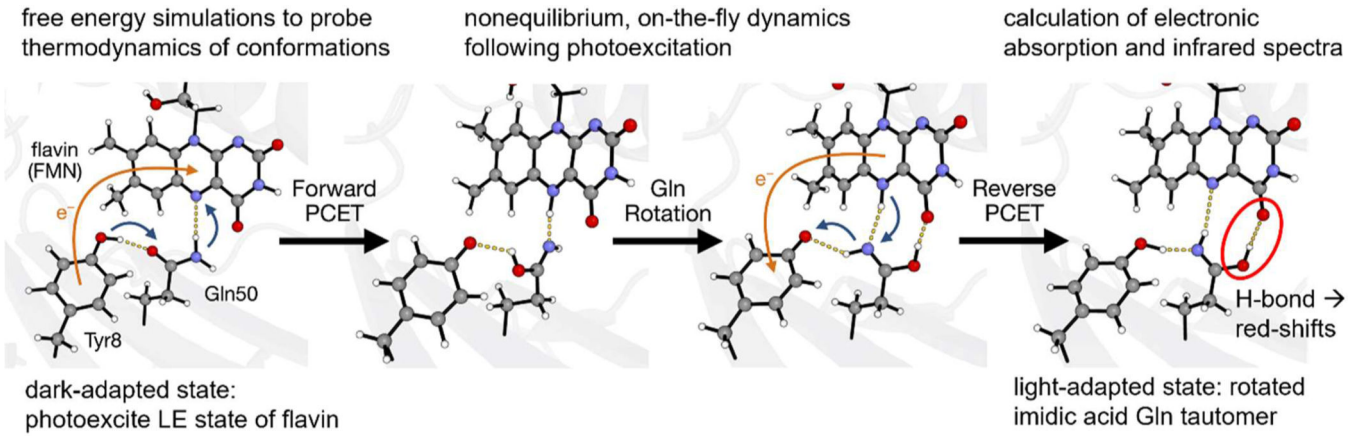

Figure 5:

Proposed photocycle of the Slr1694 BLUF photoreceptor protein based on nonequilibrium real-time dynamics simulations. Electron transfer is indicated by the orange arrow, and double proton transfer is indicated by the blue arrows. The trajectories were equilibrated in the ground state, and the photocycle was initiated by photoexcitation to the local excited state of the flavin. The light-adapted state is characterized by a rotated imidic acid Gln tautomer that hydrogen bonds to the C4 = O of the flavin, leading to red shifts of the computed flavin electronic absorption and C4 = O vibrational stretch, in agreement with experimental measurements. Comparison of computational and experimental data is important for validation of the computational models and methods. The atoms are carbon (gray), hydrogen (white), nitrogen (blue), and oxygen (red). Figure adapted with permission from Ref. [9].

Author Manuscript Author Manuscript Author Manuscript Author Manuscript